Journal of Magnetic Resonance 237 (2013) 158–163

Contents lists available at ScienceDirect

Journal of Magnetic Resonance

journal homepage: www.elsevier.com/locate/jmr

Communication

Ultralow field NMR spectrometer with an atomic magnetometer near room temperature

Guobin Liu, Xiaofeng Li, Xianping Sun, Jiwen Feng, Chaohui Ye, Xin Zhou *

Key Laboratory of Magnetic Resonance in Biological Systems, State Key Laboratory of Magnetic Resonance and Atomic and Molecular Physics, Wuhan Center for Magnetic Resonance, Wuhan Institute of Physics and Mathematics, Chinese Academy of Sciences, Wuhan 430071, China

ARTICLE INFO

Article history:
Received 4 July 2013
Revised 13 October 2013
Available online 28 October 2013

Keywords:
Atomic magnetometer
Ultralow field NMR
Near room temperature
Fast sampling

ABSTRACT

We present a Cs atomic magnetometer with a sensitivity of 150 fT/Hz$^{1/2}$ operating near room temperature. The nuclear magnetic resonance (NMR) signal of 125 μL tap water was detected at an ultralow magnetic field down to 47 nT, with the signal-to-noise ratio (SNR) of the NMR signal approaching 50 after eight averages. Relaxivity experiments with a Gd(DTPA) contrast agent in zero field were performed, in order to show the magnetometer's ability to measure spin–lattice relaxation time with high accuracy. This demonstrates the feasibility of an ultralow field NMR spectrometer based on a Cs atomic magnetometer, which has a low working temperature, short data acquisition time and high sensitivity. This kind of NMR spectrometer has great potential in applications such as chemical analysis and magnetic relaxometry detection in ultralow or zero fields.

1. Introduction

As a versatile analytical technique, nuclear magnetic resonance (NMR) has been used not only in fundamental research in physics, chemistry and biology, but also for practical applications such as medical imaging and oil well logging [1]. However, the poor sensitivity of conventional inductive pick-up coils at low frequency hinders many possible applications, and hence most endeavors in enhancing sensitivity focus on high-field NMR.

Optical atomic magnetometers, which are usually operated at low magnetic field (i.e., at the Earth's field, or even lower), provide an alternative approach for low-field NMR. Unlike a pick-up coil in conventional NMR, an atomic magnetometer is particularly sensitive in the frequency range from DC to a few kilohertz. In addition, it does not require the cryogenics that are needed by the superconducting magnets used in a high-field NMR spectrometer (although electromagnets can realize magnetic fields higher than 25 T, they cannot fulfill the requirements of stability and homogeneity for NMR spectrometers with working frequency higher than 100 MHz), or by magnetic sensors based on a superconducting quantum interference device (SQUID). Therefore, magnetometers show great potential to provide a highly sensitive and inexpensive analytical tool for low- or ultralow-field NMR [2].

Although the first NMR detection with atomic magnetometer dates back to the late 1960s [3], within the last decade there has been a revival of research interest in laser-detected NMR based on high-sensitivity atomic magnetometers. Savukov et al. performed NMR detection with a spin-exchange relaxation-free (SERF) atomic magnetometer [4]. Due to the high sensitivity (20 fT/Hz$^{1/2}$) of the SERF atomic magnetometer, single-shot nuclear magnetic resonance (NMR) sampling is possible and the signal-to-noise ratio (SNR) of the obtained NMR spectrum is acceptable. Ledbetter et al. detected *J* coupling spectra of ^{13}C enriched methanol at zero magnetic field [5] and experimentally demonstrated that zero-field NMR with an atomic magnetometer is adequate to perform structural analysis for molecules [6]. Xu et al. realized a low-temperature atomic magnetometer and used it to image flowing water [7,8]. They realized relatively high-frequency detection of the NMR signal due to the higher temporal resolution afforded by a remote detection scheme. However, this method increase the time needed to acquire an NMR signal because remote detection usually uses phase encoding rather than frequency encoding, and a seriously broadened NMR spectral line was observed due to the dispersion of water while flowing in the tube, as discussed in Ref. [7].

Usually, atomic magnetometers used for NMR detection need to work in the SERF region (an exception is the RF atomic magnetometer, which works in a partially realized SERF region, see Ref. [9] and reference therein), implying a high working temperature (above 170 °C) [4–6]. The magnetic field $\boldsymbol{B}_s$, produced by the sample and detected by the magnetometer, decreases with r^3, where r is the distance between the sample and magnetometer. Normally, r is on the order of one centimeter so as to realize a high filling factor between the magnetometer vapor cell and the magnetized sample. In this case, the high-temperature detector would heat the sample to some extent and cause faster relaxation of the sample

* Corresponding author. Fax: +86 27 87199291.
E-mail address: xinzhou@wipm.ac.cn (X. Zhou).

1090-7807/$ - see front matter © 2013 Elsevier Inc. All rights reserved.
http://dx.doi.org/10.1016/j.jmr.2013.10.008

magnetization, thus lowering the sensitivity. In particular, for a sample with a lower boiling point, the high temperature of the magnetometer cell might cause instability [10] or even vaporization, resulting in an undetectable NMR signal. Thermal isolation could be used in such an atomic magnetometer, but it cannot completely remove the thermal effect.

Here, we report an atomic magnetometer utilizing nonlinear magneto-optical rotation (NMOR) of Cs atoms near room temperature (40 °C), which reaches a sensitivity of 150 fT/Hz$^{1/2}$. It is able to detect the NMR signal of tap water with an SNR comparable to that realized by high-temperature SERF magnetometers [5,6]. The linewidth is narrowed to a value favorable for NMR spectroscopy applications, and the NMR spectrum is achieved within an acquisition time of less than 6 min.

2. Experiment and methods

2.1. The high-sensitivity Cs atomic magnetometer

An atomic magnetometer was built based on the NMOR effect, with experimental details shown in Fig. 1. Firstly, a five-layer mu-metal shield was constructed to magnetically shield the geomagnetic field by a factor of about 10^5, leaving a residual field below 1 nT. In addition to the magnetic shield, several sets of coils were used to balance the residual magnetic field gradient inside the shield. By fine-tuning the current in the coils, the residual field effect can be further minimized.

Cesium was used as the magnetometer medium. A small droplet of cesium metal was enclosed in a 1 cm cubic glass cell, which was coated with paraffin following a standard process including vacuum pumping, oven baking and evaporating paraffin, etc. [11]. The coating reduces the relaxation rate of cesium atoms by preventing them from losing angular momentum during collisions with the cell wall [12]. A resistance heater controlled the temperature of the vapor cell, and the heating current was modulated using a standard PID (proportional, integral, derivative) program. The current was on the order of several hundred milli-amperes and created a magnetic field large enough to disturb the sample spin precession, so it was turned off during NMR signal acquisition. The temperature of the Cs atoms was stabilized at 40 °C, relatively close to room temperature.

A single resonant laser beam was used for both pumping and probing the cesium atoms. The laser frequency was locked to the Cs D1 line (895 nm) by the saturated absorption spectra (SAS). The laser beam was shaped, optically isolated, intensity filtered, and linearly polarized by the optics before entering the vapor cell. The transmitted laser light was analyzed by a polarimeter and detected with a balanced photodetector.

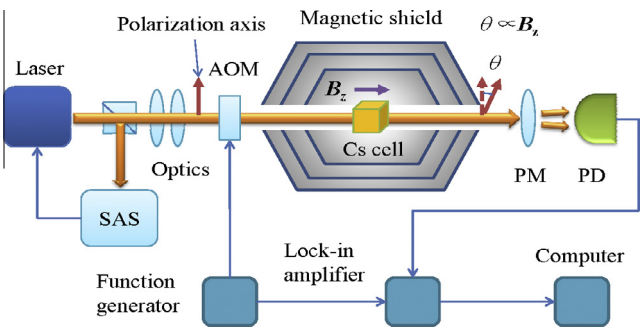

Fig. 1. The experimental details of the atomic magnetometer based on the NMOR effect. SAS: saturated absorption spectra; AOM: acoustic-optical modulator; PM: polarimeter; PD: photodetector.

The rotation angle of the polarization plane of the laser light, i.e. θ, shown in Fig. 1, was detected as the difference between the intensities of the two output beams of the polarimeter (PM). In the presence of $\boldsymbol{B_z}$, i.e. the magnetic field component in the direction of laser propagation, the rotation angle θ is proportional to it with a high proportionality ratio, in the field range corresponding to the linewidth of NMOR resonance [13]. Since the NMOR resonance width can be narrowed down to a few tens of hertz, the magnetometer can readily measure weak magnetic fields with high sensitivity.

In order to achieve a discriminator signal with large enough slope for measuring the sample magnetization, the laser was amplitude modulated by an acoustic optical modulator (AOM), and the output signal of the photodetector was processed with a lock-in amplifier (LIA) referenced to the AOM modulation frequency [14]. The LIA improved the SNR of the discriminator signal. A set of experimentally realized NMOR signals output from the LIA is illustrated in Fig. 2, wherein the in-phase signal was employed as the discriminator signal for the detection of NMR sample magnetization.

The ability of an atomic magnetometer to sense magnetic fields is generally characterized by the sensitivity, which is determined by the SNR and linewidth of the discriminator signal through the following equation:

$$\delta B = \frac{\Delta v}{\gamma_\alpha \mathrm{SNR}} \tag{1}$$

where γ_a is the gyromagnetic ratio of the alkali metal, Δv is the linewidth, and δB is the minimum magnetic field that can be discriminated by the atomic magnetometer.

The smaller δB is, the higher sensitivity is. In order to maximize the sensitivity, one should minimize the linewidth Δv and increase the SNR simultaneously. Unfortunately, for alkali atoms working at low temperature, Δv normally increases together with SNR as the temperature rises, forcing a compromise in optimizing Δv and SNR. According to our experiments, 40 °C was found to be a good value for the cesium vapor cell. Without notable loss of SNR, the linewidth of the NMOR signal obtained at this temperature could be narrowed down to 40 Hz, which was equivalent to 12 nT for cesium atoms. Compared to the 15 nT linewidth of the hot rubidium cell (170 °C) reported in Ref. [5], our experimental linewidth is narrower. This is probably due to a good coating, as the literature reported that the SERF magnetometer could also be realized at low temperature [15].

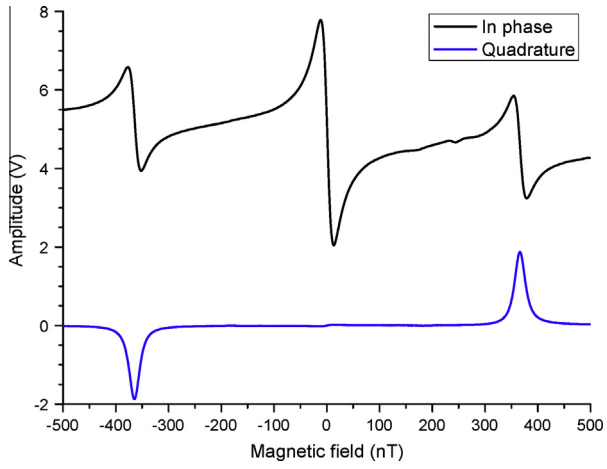

Fig. 2. The NMOR signals output from the in-phase and quadrature channels of the lock-in amplifier. The in-phase signal is shifted from the zero baseline to avoid superposition with the quadrature signal.

Fig. 3 shows the observed sensitivity of our atomic magnetometer, which was determined from the frequency-dependent magnetic noise floor converted from the LIA in-phase output noise voltage. The result is an average of 10 acquisitions with 10 kHz sampling rate. The 50 Hz signal and its harmonics are due to the power line noise. Our atomic magnetometer reaches a sensitivity of 150 fT/Hz$^{1/2}$ at the frequency range from near 10 Hz to 500 Hz ($1/f$ noise worsens the sensitivity below 10 Hz). This is less sensitive than the double-cell Cs atomic magnetometer (80 fT/Hz$^{1/2}$) reported in Ref. [16], but our setup is greatly simplified due to the single vapor cell.

As far as we know, the sensitivity achieved here is unsurpassed among single-cell Cs atomic magnetometers working at similar temperatures. There was a more sensitive version of Cs magnetometer, but it operates at a temperature of 103 °C [17]. It is worth indicating that the 40 Hz linewidth of the in-phase NMOR signal observed here is not superior to that of the SERF magnetometer in Ref. [17]. The unsurpassed sensitivity of our atomic magnetometer (compared with the products of same category) is mainly attributed to a large SNR, as indicated by the NMOR signals shown in Fig. 2. The SNR improvement also ensures a high quality of the NMR signal with few averages, as will be shown later.

2.2. The laser-detected NMR equipment

Fig. 4 shows a schematic of our atomic magnetometer for NMR detection at the ultralow field, with one-quarter of the magnetic shield (the bulk in gray in Fig. 4) cut out to expose the interior elements. The equipment includes two major parts: One is the atomic magnetometer, as described previously, serving as the magnetic sensor for NMR detection. The other part is the system for sample pre-polarization using a permanent magnet and shuttling from the magnet into the magnetometer. The pre-polarization and detection were performed spatially separately, i.e., at the outside and inside of the magnetic shield, respectively.

As described above, the NMOR atomic magnetometer built here is primarily sensitive to a static or slowly varying magnetic field, more specifically to the z-component $\boldsymbol{B_z}$ of the magnetic field inside the Cs vapor cell as shown in Fig. 4. In the presence of an ultralow magnetic field in the X direction, the sample magnetization's Larmor precession produces a low-frequency (several hertz to a few hundred hertz) alternating magnetic field $\boldsymbol{B_s}$, whose projection on the Z direction can be monitored by the atomic magnetometer. As a result, the magnetometer can detect the alternating NMR signal in an ultralow magnetic field.

The pre-polarization is performed using a Halbach magnet. With a compact ring design, the magnet has a radial magnetic field B_0 of about 1.3 T, with inhomogeneity of about 1% in the region of a $\varnothing 10 \times 10$ mm. Since the pre-polarization and detection are performed in different locations, this inhomogeneous field does not cause any direct line broadening in the detected NMR spectra. The economic permanent magnet tremendously cut down the costs compared to the typical superconducting magnet.

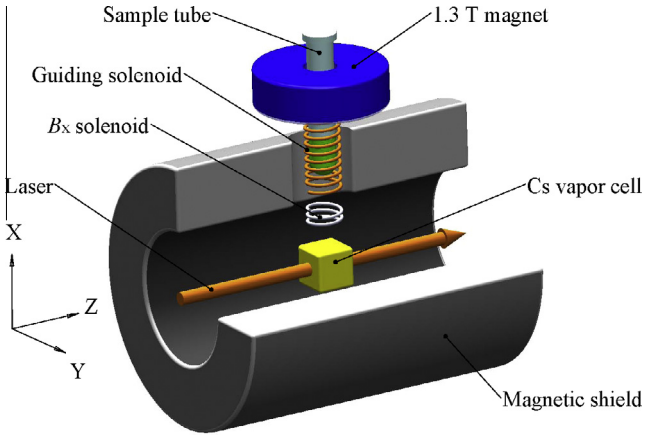

Fig. 4. Laser-detected NMR based on the Cs atomic magnetometer working near room temperature. The pre-polarization and precession of sample spins both occur in the YZ plane. Once the sample is pre-polarized by a 1.3 T permanent magnet located outside of the magnetic shield, the pre-polarized sample is then pneumatically shuttled down to the atomic magnetometer for NMR detection.

The atomic magnetometer sensor is immobilized at the center of the magnetic shield, and the sample is pre-polarized outside the shield. Therefore, a shuttling system to transport the sample tube into the shield is required. Spin magnetization of a liquid sample such as tap water generally decays on a timescale of hundreds of milliseconds to a few seconds, which necessitates that the shuttling time of the sample be less than a few hundred milliseconds.

We designed and realized the sample pneumatic shuttling system by using electromagnetic valves, air compressors and some glass tubes. The shuttling time is controllable by the air pressure driving the sample tube, and it can be as short as 100 ms. In order to minimize sample depolarization during the transportation, a magnetic field of about one gauss produced by a guiding solenoid is used. However, no obvious signal attenuation was observed in experiments without the guiding field. This might be attributed to the short shuttling time.

The procedure to obtain an NMR signal is as follows: first, pre-polarize the sample for a time of about 3–5T_1, then shuttle the sample tube into the atomic magnetometer within three hundred milliseconds, and finally detect the NMR signal while applying the $\boldsymbol{B_x}$ field. It should be noted that the finite length of the transverse solenoid ($\boldsymbol{B_x}$ solenoid as shown in Fig. 4) and the gap (around 15 mm) between the Cs cell and $\boldsymbol{B_x}$ solenoid caused leakage of the

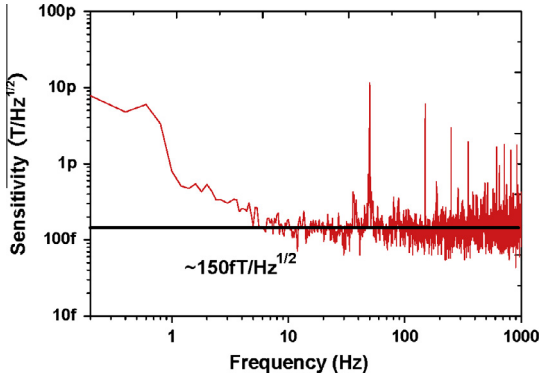

Fig. 3. The frequency dependence of sensitivity of the atomic magnetometer.

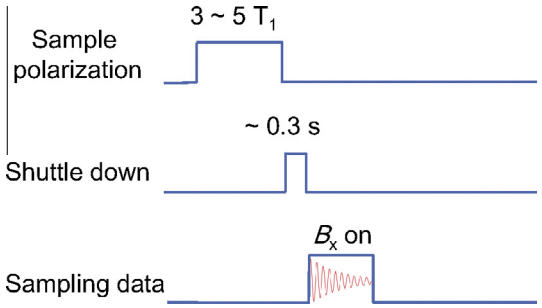

Fig. 5. The timing sequence for NMR acquisition in a laser-detected NMR experiment. The guiding solenoid is powered on during the shuttle-down time. Total time for one sampling is about 6–10T_1.

transverse field, so that the linewidth of the NMOR resonance was broadened to several times that of the unperturbed resonance. Therefore, it is necessary to cancel out this broadening by tuning the balance coils once again before an NMR measurement. While the transverse field is relatively small (several tens of nT in our case), the cancelation is good. The data were recorded at a sampling rate of 1 kHz by a PCI card. A Labview program controlled all operations, and the timing sequence is shown in Fig. 5. The most important difference between our spectrometer and a conventional NMR spectrometer is that the pre-polarization and precession of sample spins occur both in the *YZ* plane, and the magnetic sensor is sensitive to the magnetic field in the *Z* direction, so the usual $\pi/2$ tipping pulse is unnecessary in the sampling process.

3. Results and discussion

3.1. NMR detection of tap water at ultralow field

An NMR signal of tap water with an average of eight samplings is plotted in Fig. 6a, with baseline drift subtracted in data processing. Fig. 6b is the corresponding NMR spectrum processed by the discrete Fourier transformation (DFT). The central frequency of the NMR signal is 2 Hz, corresponding to an ultralow magnetic field of 47 nT.

The value of T_2^* obtained from the fit of Fig. 6a is 1.1 s, giving a linewidth of 0.32 Hz. The linewidth consists of two parts. One is the broadening due to an inhomogeneous magnetic field produced by the homebuilt solenoid. Based on our simulations, the solenoid ($\varnothing 20 \times 18$ mm) produces a magnetic field of 47 nT with $\Delta B = 5$ nT deviation over the volume of sample. This would cause 0.2 Hz line broadening given the equation $\Delta v = \gamma_p \Delta B$. The residual linewidth

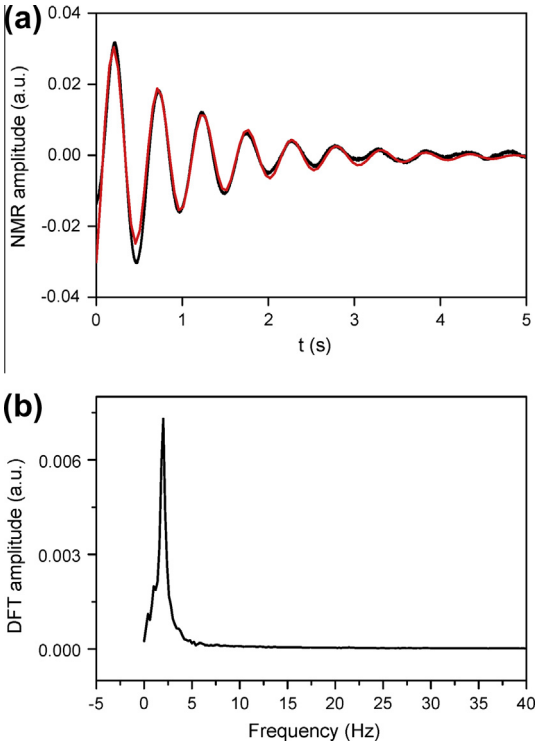

Fig. 6. (a) The NMR signal with an average of eight samplings and (b) its NMR spectrum processed with the DFT. In (a), the red curve shows a fitting of the NMR signal, from which the value of T_2^* was determined to be 1.1 s. (For interpretation of the references to color in this figure legend, the reader is referred to the web version of this article.)

of 0.12 Hz means a T_2 of 2.6 s, which is a reasonable value for protons in tap water.

According to the experimental results in Ref. [5], a linewidth of 0.1 Hz is possible at zero magnetic field, which means there is still room for narrowing the spectral line in our case. A further improvement on this is necessary when characterizing complicated samples, such as those having carbon–hydrogen bonds, wherein the complex and crowded (spectra interval between neighbor peaks is usually 0.5 Hz or even smaller) *J*-coupling multiplets in low field need to be discriminated [18].

The single-shot time to obtain each NMR signal includes the durations for pre-polarizing the sample, shuttling the tube, and sampling data, as per the timing sequence shown in Fig. 5. The pre-polarization time amounts to half the total, and therefore the single-shot time is on the order of $6–10T_1$. For most NMR samples, the single-shot time is usually less than 1 min. Experimentally, the single-shot time for the tap water NMR sampling performed here was less than 40 s.

Repeated sampling was performed to further increase the SNR. We found in our experiments that only a few repetitions were necessary. The NMR signal displayed in Fig. 6a is from an average of 8 samplings and took less than 6 min. Considering the NMR amplitude and noise floor in Fig. 6b, the SNR reaches 50 or even higher for the 125 μL sample volume of tap water, better than that reported in Ref. [4] and comparable to the results in Refs. [5,6]. However, the experimental results reported here were obtained with a shorter acquisition time and a lower temperature compared to the work in Refs. [5,7,8] and Refs. [4,6], respectively.

Concerning practical NMR applications, the two most important parameters of a spectrometer are the signal's linewidth and SNR. The result obtained here shows that the linewidth is moderate and improvable, and the SNR is adequate for chemical analysis based on NMR spectroscopy. Although the obtained SNR is mostly due to the relatively high molar concentration of protons in tap water, it is easy to increase the degree of polarization of samples other than water by applying hyperpolarization technologies, such as para-hydrogen induced polarization (PHIP) [6], laser-polarized xenon using optical pumping [19] and dynamic nuclear polarization [20], since the simple configuration of the laser-detected NMR spectrometer realized here makes it very compatible with many other equipments. In such cases, the permanent magnet in Fig. 4 would not be necessary.

Nevertheless, there is room for improving the equipment. For example, the broad base of the NMR signal, as seen in Fig. 6b, is mainly due to the presence of near-zero-frequency components and caused by long-timescale drifts of various parameters of the different materials used in the equipment; this can be decreased by artificial aging of materials under special conditions.

In conclusion, we experimentally demonstrated a fast data acquisition laser-detected NMR spectrometer based on a low temperature atomic magnetometer. Such an atomic magnetometer working near room temperature will make the spectrometer favorable in biological and medical usage where long diagnosis time is unacceptable or samples are sensitive to high temperature.

3.2. Relaxivity detection of gadolinium complexes at zero field

To show another application, we also use the atomic magnetometer to detect the relaxivity of a gadolinium based contrast agent. Gadolinium complexes increase the T_1 relaxation rate of nearby water and thus enhance the imaging contrast of targeting tissues. Of various gadolinium complexes, Gd(DTPA) is a widely used contrast agent for MRI diagnosis in hospitals. Relaxivity detection of Gd(DTPA) with an atomic magnetometer was reported previously using a remote detection scheme [21]. Although the

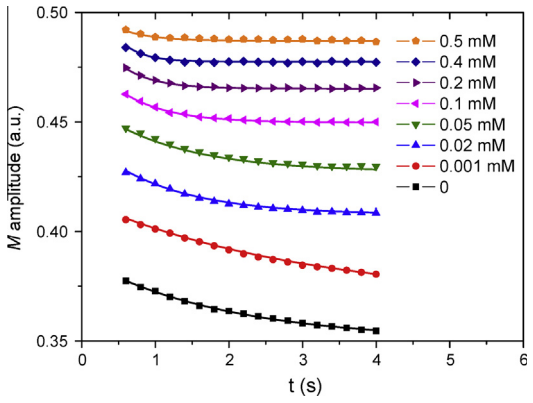

Fig. 7. T_1 decays recorded for eight different Gd(DTPA) concentrations. From 0 (lowest curve) to 0.5 mM (top curve), an increasing decay rate is observed.

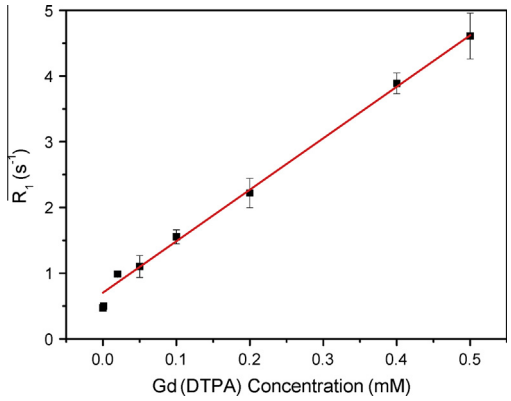

Fig. 8. The relaxation rate R_1 as a function of the concentration of the contrast agent Gd(DTPA). The linear fit (red line) gives a relaxivity of $7.8 \pm 0.12\ s^{-1}\ mM^{-1}$. (For interpretation of the references to color in this figure legend, the reader is referred to the web version of this article.)

detection limit of the remote detection geometry is lower, it takes a longer time to obtain each sampling.

Eight different Gd(DTPA) concentrations were studied in our experiment: 0 (deionized water only), 0.001, 0.02, 0.05, 0.1, 0.2, 0.4 and 0.5 mM, respectively. The T_1 decays of the eight sample magnetizations were recorded as shown in Fig. 7. In zero magnetic field, there is no Larmor precession, so the atomic magnetometer records directly the longitudinal z-component of sample's exponentially decaying magnetization. Prior to each experiment, the direction of the B_0 field was adjusted to maximize the initial magnetization of the sample after shuttling. The data were recorded continuously in a single shot, but each decay curve is shown with discrete points for clarity. This experiment required much less sampling time compared to the remote detection scheme.

Fig. 8 shows the dependence of the spin–lattice relaxation rate $R_1(1/T_1)$ on the concentration of Gd(DTPA). According to the following relation,

$$R_2 = R_1(0) + \alpha C \tag{2}$$

where C represents concentration of the contrast agent, $R_1(0)$ is the relaxation rate in absence of the contrast agent, and α is the relaxivity. A linear fit of the data, as shown in Fig. 8, gives a relaxivity of $7.84 \pm 0.12\ s^{-1}\ mM^{-1}$, which is consistent with the result obtained from a field-cycling measurement at low field [22].

Although this relaxivity measurement experiment is just a demonstration, the low-temperature atomic magnetic field sensor shows a high accuracy in contrast agent-enhanced T_1 measurement. This indicates great potential for application to the medical imaging methodology proposed by Savukov et al. in Ref. [4].

4. Conclusion

We realized an atomic magnetometer with a sensitivity of $150\ fT/Hz^{1/2}$ at the frequency range from near 10 Hz to 500 Hz, which was used to detect the NMR signal of tap water at an ultralow magnetic field of 47 nT with moderate linewidth and SNR. This laser-detected NMR spectrometer, based on the NMOR atomic magnetometer, employs only one low-cost permanent magnet and does not require any cryogenics.

If integrated with advanced manufacture technology, such as micro-electromechanical systems (MEMS) [23], the atomic magnetometer could be mass-produced. An array of atomic magnetometers working in a magnetically shielded environment at room temperature is well-suited for fast medical diagnosis and imaging, with applications including magnetocardiography (MCG) and magnetoencephalography (MEG).

Although there have been several ultralow- or zero-field NMR experiments conducted with atomic magnetometers [5–9], the potential for other applications, such as detection of magnetic particles [24], has not been fully explored. It was recently shown that an atomic magnetometer can be used for magnetic relaxometry measurements of nanoparticle-labeled cancer cells [25]. As a high-sensitivity detector for magnetic relaxometry, an atomic magnetometer is advantageous and less expensive compared to the regularly used SQUID sensors because of lack of cryogenics.

In conclusion, we constructed and experimentally demonstrated an ultralow-field NMR spectrometer based on a Cs atomic magnetometer near room temperature. Without significantly sacrificing the SNR, the fast sampling and low-temperature operation make the spectrometer particularly favorable for biological and medical applications. Our relaxivity measurements of Gd(DTPA) indicates that our atomic magnetometer is suitable for such relaxometry studies.

Acknowledgments

This work was supported by the Natural Science Foundation of China (81227902, 11004228, 11305256), the Innovation Method Fund of China (2010IM030600), and the Chinese Academy of Sciences (the 100 talents program and KJCX2-EW-N06-04). The authors would like to thank Xiuchao Zhao for helping the test of SAS optics and thank Xiaoxiao Zhang for preparing the Gd(DTPA) samples. Guobin Liu and Xin Zhou also would like to thank Dr. Scott Seltzer for editing the manuscript and giving helpful advice.

References

[1] B. Blumich, J. Perlo, F. Casanova, Mobile single-sided NMR, Prog. Nucl. Magn. Reson. Spectrosc. 52 (2008) 197.
[2] D. Budker, M.V. Romalis, Optical magnetometry, Nat. Phys. 3 (2007) 227.
[3] C. Cohen-Tannoudji, J. Dupont-Roc, S. Haroche, F. Laloe, Phys. Rev. Lett. 22 (1969) 758.
[4] I.M. Savukov, M.V. Romalis, NMR detection with an atomic magnetometer, Phys. Rev. Lett. 94 (2005) 123001.
[5] M.P. Ledbetter, C.W. Crawford, A. Pines, D.E. Wemmerb, S. Knappe, J. Kitching, D. Budker, Optical detection of NMR J-spectra at zero magnetic field, J. Magn. Res. 199 (2009) 25.
[6] T. Theis, P. Ganssle, G. Kervern, S. Knappe, J. Kitching, M.P. Ledbetter, D. Budker, A. Pines, Parahydrogen-enhanced zero-field nuclear magnetic resonance, Nat. Phys. 7 (2011) 571.
[7] S. Xu, S.M. Rochester, V.V. Yashchuk, M.H. Donaldson, D. Budker, Construction and applications of an atomic magnetic gradiometer based on nonlinear magneto-optical rotation, Rev. Sci. Instrum. 77 (2006) 083106.
[8] S. Xu, V. Yashchuk, M.H. Donaldson, S.M. Rochester, D. Budker, A. Pines, Magnetic resonance imaging with an optical atomic magnetometer, Proc. Natl. Acad. Sci. U. S. A. 103 (2006) 12668.

[9] I.M. Savukov, S.J. Selzter, M.V. Romalis, Detection of NMR signals with a radio-frequency atomic magnetometer, J. Magn. Res. 185 (2007) 214.
[10] M.P. Ledbetter, I.M. Savukov, D. Budker, V. Shah, S. Knappe, J. Kitching, D.J. Michalak, S. Xu, A. Pines, Zero-field remote detection of NMR with a microfabricated atomic magnetometer, Proc. Natl. Acad. Sci. U. S. A. 105 (2008) 2286.
[11] E.B. Alexandrov, M.V. Balabas, D. Budker, D. English, D.F. Kimball, C.-H. Li, V.V. Yashchuk, Phys. Rev. A 66 (2002) 042903.
[12] M.A. Bouchiat, J. Brossel, Relaxation of optically pumped Rb atoms on paraffin-coated walls, Phys. Rev. 147 (1966) 41.
[13] D. Budker, V.V. Yashchuk, M. Zolotorev, Nonlinear magneto-optic effects with ultranarrow widths, Phys. Rev. Lett. 81 (1998) 5788.
[14] W. Gawlik, L. Krzemien, S. Pustelny, D. Sangla, J. Zachorowski, M. Graf, A.O. Sushkov, D. Budker, Nonlinear magneto-optical rotation with amplitude modulated light, Appl. Phys. Lett. 88 (2006) 131108.
[15] M.V. Balabas, T. Karaulanov, M.P. Ledbetter, D. Budker, Polarized alkali-metal vapor with minute-long transverse spin-relaxation time, Phys. Rev. Lett. 105 (2010) 070801.
[16] N.C. Garcia, D. Yu, L. Yao, S. Xu, Optical atomic magnetometer at body temperature for magnetic particle imaging and nuclear magnetic resonance, Opt. Lett. 35 (2010) 661.
[17] M.P. Ledbetter, I.M. Savukov, V.M. Acosta, D. Budker, M.V. Romalis, Spin-exchange-relaxation-free magnetometry with Cs vapor, Phys. Rev. A 77 (2008) 033408.
[18] S. Appelt, F.W. Hasing, U. Sieling, A. Gordji-Nejad, S. Gloggler, B. Blumich, Paths from weak to strong coupling in NMR, Phys. Rev. A 81 (2010) 023420.
[19] X. Zhou, D. Graziani, A. Pines, Hyperpolarized xenon NMR and MRI signal amplification by gas extraction, Proc. Natl. Acad. Sci. U. S. A. 106 (2009) 16903.
[20] J.H. Ardenkjær-Larsen, B. Fridlund, A. Gram, G. Hansson, L. Hansson, M.H. Lerche, R. Servin, M. Thaning, K. Golman, Increase in signal-to-noise ratio of >10,000 times in liquid-state NMR, Proc. Natl. Acad. Sci. U. S. A. 100 (2003) 10158.
[21] D.J. Michalak, S. Xu, T.J. Lowery, C.W. Crawford, M. Ledbetter, L. Bouchard, D.E. Wemmer, D. Budker, A. Pines, Relaxivity of gadolinium complexes detected by atomic magnetometry, Magn. Reson. Med. 66 (2011) 605.
[22] P. Caravan, Strategies for increasing the sensitivity of gadolinium based MRI contrast agents, Chem. Soc. Rev. 35 (2006) 512.
[23] V. Shah, S. Knappe, P.D.D. Schwindt, J. Kitching, Subpicotesla atomic magnetometry with a microfabricated vapour cell, Nat. Photon. 1 (2007) 649.
[24] D. Maser, S. Pandey, H. Ring, M.P. Ledbetter, S. Knappe, J. Kitching, D. Budker, Detection of a single cobalt microparticle with a microfabricated atomic magnetometer, Rev. Sci. Instrum. 82 (2011) 086112.
[25] C. Johnson, N.L. Adolphi, K.L. Butler, D.M. Lovato, R. Larson, P.D.D. Schwindt, E.R. Flynn, Magnetic relaxometry with an atomic magnetometer and SQUID sensors on targeted cancer cells, J. Magn. Magn. Mater. 324 (2012) 2613.